Efficient POPS-OFDM Waveform Design for Future Wireless Communication Systems

Zeineb Hraiech, Mohamed Siala, Fatma Abdelkefi, and Tuncer Baykas

***Abstract*—Future wireless networks are required to offer new applications and services, which will experience high dispersions in time and frequency, incurred mainly by coarse synchronization. Coarse synchronization is induced by signaling overhead reduction and dictated by the tremendous optimization of the radio interface efficiency. It is expected to dramatically damage waveform orthogonality in conventional orthogonal frequency-division multiplexing (OFDM) systems and to result in oppressive intercarrier interference (ICI). To alleviate the degradation in performance caused by ICI, the concept of nonorthogonal multiplexing has been promoted, as a serious alternative to strict orthogonal multiplexing, for guaranteeing the OFDM benefits without requiring high-level synchronization. Within this nonorthogonal multiplexing framework, ping-pong optimized pulse shaping-OFDM (POPS-OFDM) has been introduced as a powerful tool to efficiently design waveforms, which withstand future multicarrier systems' dispersion impairments. In this paper, we investigate the discrete time version of the POPS-OFDM approach and study its sensitivity and robustness against estimation and synchronization errors. Based on numerical results, we show that POPS-OFDM provides an important gain in the signal-to-interference ratio, typically higher than 5 dB, with respect to conventional OFDM. We also demonstrate that POPS-OFDM brings an increased robustness against synchronization errors and ensures a dramatic reduction in out-of-band emissions, enabling flexible and improved spectrum utilization.**

***Index Terms*—Intercarrier interference (ICI), intersymbol interference (ISI), out-of-band (OOB) emissions, ping-pong optimized pulse shaping-OFDM (POPS-OFDM), signal-to-interference-plus-noise ratio (SINR), waveform design.**

I. Introduction

TO MEET the future communication services and needs that are looming on the horizon, the transition to the next fifth generation (5G) of mobile communication systems is becoming a must further essential [1]. First and foremost, the trend to offer novel applications of wireless communication certainly imposes new challenges, ranging from reduced latency to high robustness to synchronization errors and misalignments in time and frequency. Among those applications, Tactile Internet [1]–[3], which comprises real-time applications with extremely low latency requirements, imposes a time budget on the physical layer below 100 μs [2]–[4]. In addition, machine-type communication [3], [5], which generates sporadic traffic and has quite limited processing capabilities, needs to be coarsely synchronized to guarantee long battery lifetimes. Unfortunately, orthogonal frequency-division multiplexing (OFDM), adopted by the 4G standard, is not suitable for the above applications, since it requires strict synchronism and perfect waveform orthogonality [5]. To ensure that, the OFDM technique necessitates a huge overhead in the spectrum and energy resources and leads to a dramatic increase in latency, which is brought by signaling and transmission of training sequences [6]. In this framework, coarse synchronization emerges as a key solution, since it reduces the signaling load and keeps it within tolerable and acceptable levels. However, relaxing synchronicity can dramatically damage the OFDM signals and most likely result in unbearable intercarrier interference (ICI) and intersymbol interference (ISI). Therefore, the main focus is to find a system based on nonorthogonal wireless multicarrier schemes, with well-localized waveforms in time and frequency domains. These waveforms should be robust to relaxed time/frequency synchronization requirements expected in several future 5G applications.

One of the alternative access techniques envisaged for 5G is referred to as generalized frequency-division multiplexing (GFDM) [3], [7], [8]. Compared to conventional OFDM, GFDM offers a low out-of-band (OOB) emissions, thanks to an adjustable transmit pulse shaping filter, which is applied to individual subcarriers. This technique requires the aggregation of a significant number of transmitting symbols, to which a single cyclic prefix (CP) insertion overhead is appended, in order to reduce overhead and increase spectrum and energy efficiencies. Unfortunately, GFDM, which banks on circular channel convolution and is brought by CP addition, can only work over nontime-selective channels and requires a perfect frequency synchronization at the receiver (Rx). Another candidate, under consideration for 5G, is filter bank multicarrier (FBMC) [9], [10]. FBMC also offers a high-level control of the OOB emissions, with frequency-localized shaping pulses. This scheme does not require CP, and hence, it improves the spectral efficiency [3], [11]. However, neither the low-latency requirements nor the simplicity of implementation is guaran-

Manuscript received July 26, 2017; revised March 29, 2018; accepted April 27, 2018. Date of publication May 30, 2018; date of current version February 22, 2019. The work of T. Baykas was supported by the Scientific and Technological Research Council of Turkey through Bideb 2232 Program under Grant 115C136. *(Corresponding author: Zeineb Hraiech.)*

Z. Hraiech and M. Siala are with the MEDIATRON Laboratory, Higher School of Communications, University of Carthage, 2083 Ariana, Tunisia (e-mail: zeineb.hraiech@supcom.tn; mohamed.siala@supcom.tn).

F. Abdelkefi is with the Reconfigurable and Embedded Digital Systems Institute, School of Management and Engineering Vaud, University of Applied Sciences Western Switzerland, CH-1400 Yverdon-les-Bains, Switzerland. He is also with the MEDIATRON Laboratory, Higher School of Communications, University of Carthage, 2083 Ariana, Tunisia, and also with IMT Atlantique, UMR CNRS 6285 Lab-STIC, Universit Bretagne Loire, F-29238 Brest, France (e-mail: fatma.abdelkefi@supcom.tn).

T. Baykas is with Istanbul Medipol University, 34810 Istanbul, Turkey (e-mail: tbaykas@medipol.edu.tr).

Digital Object Identifier 10.1109/JSYST.2018.2833444

teed by FBMC [6], [7]. Universal filtered multicarrier [4], [12] was also introduced as an alternative to OFDM, where a filtering operation is applied to a group of consecutive subcarriers to reduce the OOB emissions. This scheme does not need the use of CP [12], which makes it more sensitive to small time synchronization errors and misalignments than OFDM. Hence, it is expected to be unsuitable for applications demanding a relaxed time/frequency synchronization requirements. Ping-pong optimized pulse shaping-OFDM (POPS-OFDM) [13] was proposed as an attractive candidate for the optimization of the future wireless communication systems. This innovative technique guarantees more resilience to orthogonality losses incurred by asynchronism and misalignment, since it has the advantage to bank on a nonorthogonal wireless multicarrier scheme, which allows the design of well-localized waveforms in both time and frequency domains [14], [15]. Through an iterative, yet offline, maximization of the signal-to-interference-plus-noise ratio (SINR), POPS-OFDM straightforwardly and promptly generates the optimized waveforms at the transmitter (Tx)/Rx sides. In addition to ICI/ISI mitigation, these waveforms are found to achieve unprecedented robustness against time/frequency synchronization errors. In [14] and [15], a continuous-time version of the POPS-OFDM algorithm is presented, where the optimized Tx/Rx waveforms are considered as linear combinations of the most localized Hermite functions. Hence, POPS algorithm consists of determining a couple of coefficient vectors that maximize the SINR for a given signal-to-noise ratio (SNR) value and for a rectangular scattering function. After determining the optimized vector of the coefficients of each filter, the optimum continuous-time Tx/Rx waveforms can then be deduced. In this paper, we analyze several characteristics of the discrete-time version of the POPS-OFDM and shed light on some of its relevant features. The main contributions of this work are mainly the following.

1) A discrete-time POPS-OFDM implementation with reduced complexity is proposed.
2) An upper bound on the SINR of the POPS-OFDM and an exact SINR expression of conventional OFDM systems are derived.
3) The performance evaluation of POPS-OFDM for different propagation conditions is provided.
4) The sensitivity of POPS-OFDM to estimation errors in the channel spreading factor and its robustness against the time and frequency synchronization errors are investigated.
5) The sensitivity of the POPS algorithm to waveform initialization is tested.

The rest of this paper is organized as follows. In Section II, we present the basic system model and specify the main notations used in this paper. In Section III, we describe the iterative discrete-time POPS-OFDM technique for the waveform design and derive the SINR expressions for both POPS-OFDM and conventional OFDM. In Section IV, we derive the upper bound of the SINR, which can be achieved by the proposed POPS-OFDM algorithm. In Section V, POPS-OFDM performances are evaluated in terms of robustness against time and frequency synchronization errors and its sensitivity to waveform initialization. Finally, Section VI is reserved for conclusions.

TABLE I
MATHEMATICAL NOTATIONS

Notation	Explanation
$\Re\{z\} = x$	Real part of the complex number $z = x + jy$
$\mathbb{E}$	Expectation operator
$\underline{\underline{V}} = [V_{pq}]_{p,q\in\mathbb{Z}}$	Doubly underlined $\underline{\underline{V}}$ refers to matrix $\underline{\underline{V}}$ with $(p,q)^{\text{th}}$ entry V_{pq}
$\underline{\underline{\Phi}}_{\nu_k}$	Hermitian matrix with $(p,q)^{\text{th}}$ entry $e^{j2\pi\nu_k T_s(q-p)}$
$\delta(i)$	Kronecker delta function returns 1 if $i = 1$ and 0 otherwise
$\underline{V} = [V_q]_{q\in\mathbb{Z}}$	Underlined $\underline{V}$ refers to vector $\underline{V}$ with q^{th} entry V_q
$\underline{\underline{I}} = [I_{pq}]_{p,q\in\mathbb{Z}}$	Identity matrix with $(p,q)^{\text{th}}$ entry $I_{pq} = \delta(p-q)$
$\sigma_p(\underline{\underline{M}})$	Time shift by p samples of matrix $\underline{\underline{M}}$, i.e. $\sigma_p(\underline{\underline{M}}) = [M_{m-p\ n-p}]_{m,n\in\mathbb{Z}}$
$\varpi(\underline{V})$	Temporal inversion of vector $\underline{V}$, i.e. $\varpi(\underline{V}) = [V_{-q}]_{q\in\mathbb{Z}}$
$.^H$	Hermitian transpose operator
$.^*$	Element-wise conjugation operator
$\odot$	Component-wise product of two vectors or matrices
$\otimes$	Kronecker product of two vectors ($\underline{X}\otimes\underline{V} = [X_q\underline{V}]_{q\in\mathbb{Z}}$)
$<\underline{U},\underline{V}>$	Hermitian scalar product of vectors $\underline{U}$ and $\underline{V}$
$\|\|\underline{V}\|\|$	Norm of a vector $\underline{V}$, $\|\|\underline{V}\|\| = \sqrt{<\underline{V},\underline{V}>}$
$\mathbb{N}$	Set of natural numbers, not including 0
$\mathbb{Z}$	Set of all integers

II. SYSTEM MODEL

This section provides preliminary concepts and notations related to the POPS-OFDM and the channel model used for waveform optimization and performance evaluation. The main mathematical notations used in this work are shown in Table I. For the POPS-OFDM at hand, as well as for conventional OFDM to be used as a benchmark, the symbol period or spacing is denoted by T, and the frequency spacing between two adjacent subcarriers is denoted by F. The transmitted signal is sampled at a sampling rate $R_s = \frac{1}{T_s}$, where T_s is the sampling period. Due to sampling, the total spanned bandwidth is equal to $\frac{1}{T_s}$, and the number of subcarriers is finite and equal to $Q = \frac{1}{FT_s}$, where $Q \in \mathbb{N}$. Therefore, adopting $[0, \frac{1}{T_s})$ as the spanned frequency band, the subcarrier frequencies are given by $mF = m/QT_s$, $m = 0, 1, \ldots, Q-1$. We choose the symbol duration as an integer multiple of the sampling period, i.e., $T = NT_s$, where $N \in \mathbb{N}$. We denote by $\Delta = \frac{1}{FT}$ the time–frequency lattice density of the studied OFDM system, which is taken below unity to be robust against impairments like dispersions in time and frequency. Hence, $\Delta = QT_s\frac{1}{NT_s} = \frac{Q}{N} \leq 1$, which means that Q is always smaller than or equal to N, and that the time–frequency lattice density is always rational. The difference $(N-Q)T_s$ accounts for the notion of guard duration in conventional OFDM. The discrete-time version of the transmitted signal is represented by the infinite vector $\underline{e} = (\ldots, e_{-2}, e_{-1}, e_0, e_1, \ldots)^T = [e_q]_{q\in\mathbb{Z}}$, where e_q is the transmitted signal sample at time qT_s. This signal can be written as $\underline{e} = \sum_{mn} a_{mn}\ \underline{\varphi}_{mn}$, where a_{mn} is the transmitted symbol at time nT and frequency mF (see Fig. 1). The vector used for the transmission of symbol a_{mn}, which results from a time shift of $nT = nNT_s$ and a frequency shift of $mF = m/QT_s$ of the transmission prototype vector $\underline{\varphi}$, can be written as

$$\underline{\varphi}_{mn} = [\varphi(q - nN)e^{j2\pi\frac{mq}{Q}}]_{q\in\mathbb{Z}}. \quad (1)$$

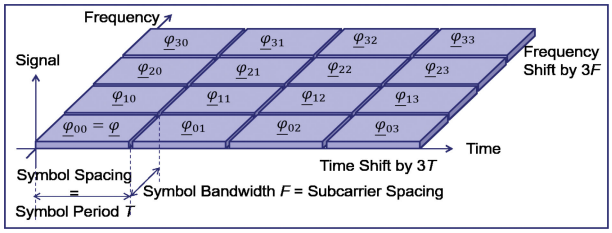

Fig. 1. Time–frequency lattice at the Tx side.

In order to get a reasonable real-time implementation in terms of processing and latency, we assume that the support duration, of the transmitted waveform, is denoted by $D_{\underline{\varphi}}$. The average energy of the transmitted symbol is denoted by $E = \mathbb{E}[|a_{mn}^2|]$. Assuming a linear time-varying multipath channel $h(p,q)$, with p and q standing, respectively, for the sampling-period normalized versions of the time delay and the normalized observation time, the discrete-time version of the received signal, $\underline{r} = [r_q]_{q\in\mathbb{Z}}$, is expressed as

$$\underline{r} = \sum_{mn} a_{mn}\underline{\widetilde{\varphi}}_{mn} + \underline{n} \tag{2}$$

where $\underline{\widetilde{\varphi}}_{mn} = [\sum_p h(p,q)\varphi_{mn}(q-p)]_{q\in\mathbb{Z}}$ is the channel-distorted version of $\underline{\varphi}_{mn}$, and $\underline{n}$ is a discrete-time and zero mean complex additive white Gaussian noise (AWGN), the samples of which are centered, uncorrelated with variance N_0. The channel is assumed compliant with wide-sense stationary uncorrelated scattering assumptions, with a finite paths' number, K, such that $h(p,q) = \sum_{k=0}^{K-1} h_k e^{j2\pi\nu_k T_s q}\delta(p-p_k)$, where h_k, ν_k, and p_k are, respectively, the amplitude, the Doppler frequency, and the time delay of the kth path. The paths' amplitudes h_k, $k = 0,\ldots,K-1$, are supposed to have zero mean and be independent random complex AWGN variables with average powers $\pi_k = \mathbb{E}[|h_k|^2]$, where $\sum_{k=0}^{K-1}\pi_k = 1$. The channel scattering function is, therefore, given by $S(p,\nu) = \sum_{k=0}^{K-1}\pi_k\delta(p-p_k)\delta(\nu-\nu_k)$. At the Rx side, the decision metric on symbol a_{kl} is given by

$$\Lambda_{kl} = \left\langle \underline{\psi}_{kl}, \underline{r}\right\rangle = \underline{\psi}_{kl}^H\,\underline{r} \tag{3}$$

where $\underline{\psi}_{kl} = [\psi(q-lN)e^{j2\pi\frac{kq}{Q}}]_{q\in\mathbb{Z}}$ is the time- and frequency-shifted version, by lT in time and kF in frequency domains, of the reception prototype vector $\underline{\psi}$. The duration of the receive waveform, denoted by $D_{\underline{\psi}}$, remains also finite in order to maintain a feasible and practical real-time implementation complexity.

III. SINR Derivation for POPS and Conventional OFDM

In this section, the discrete-time POPS-OFDM algorithm, enabling the design of optimal waveforms at the Tx/Rx sides through the SINR maximization, is presented. POPS-OFDM is an iterative algorithm, which alternates between an optimization of the receive waveform $\underline{\psi}$, for a given transmit waveform $\underline{\varphi}$, and an optimization of the transmit waveform $\underline{\varphi}$ for a given receive waveform $\underline{\psi}$. The optimization is performed offline in order to create a new waveform dictionary depending on the different channel statistics. In the practice, the suitable waveform will be selected from this dictionary to guarantee a high SINR level. Without loss of generality, we will focus on the SINR evaluation for the symbol a_{00}. Referring to (3), the decision variable on a_{00} can be expanded into three additive terms as

$$\Lambda_{00} = \underbrace{a_{00}\left\langle \underline{\psi}_{00}, \underline{\widetilde{\varphi}}_{00}\right\rangle}_{U_{00}} + \underbrace{\sum_{(m,n)\neq(0,0)} a_{mn}\left\langle \underline{\psi}_{00}, \underline{\widetilde{\varphi}}_{mn}\right\rangle}_{I_{00}} + \underbrace{\left\langle \underline{\psi}_{00}, \underline{n}\right\rangle}_{N_{00}} \tag{4}$$

where U_{00} results from the symbol to be detected, I_{00} is the ISI, accounting for both ISI and ICI, and N_{00} is the noise term. The following section will be dedicated to derive the exact closed-form expression of the SINR, which depends on the powers of U_{00}, I_{00}, and N_{00}.

A. Average Power From the Target Symbol

For a given realization of the channel, the average power from the target symbol, a_{00}, is given by $P_S^h = \frac{E}{||\underline{\varphi}||^2}\,|<\underline{\psi}_{00}, \underline{\widetilde{\varphi}}_{00}>|^2$. Therefore, the average of the useful power over all possible channel realizations is $P_S = \mathbb{E}[P_S^h]$. Under the previous notions, we deduce that

$$P_S = E\,\frac{\underline{\psi}^H\,\underline{\underline{KS}}^{\underline{\varphi}}_{S(p,\nu)}\,\underline{\psi}}{||\underline{\varphi}||^2} \tag{5}$$

where $\underline{\underline{KS}}$ refers to the Kernel matrix of the target symbol, and it has the following expression:

$$\begin{aligned}\underline{\underline{KS}}^{\underline{\varphi}}_{S(p,\nu)} &= \sum_{k=0}^{K-1}\pi_k\,\sigma_{p_k}\left(\underline{\varphi}_{00}\underline{\varphi}_{00}^H\right)\odot\underline{\underline{\Phi}}_{\nu_k}\\ &= \sum_{k=0}^{K-1}\pi_k\,\sigma_{p_k}\left(\underline{\varphi}\underline{\varphi}^H\right)\odot\underline{\underline{\Phi}}_{\nu_k}.\end{aligned} \tag{6}$$

Given that $P_S > 0$, we can state that the Kernel matrix is a positive Hermitian matrix. POPS-OFDM is conceived as an iterative algorithm, where $\underline{\psi}$ and $\underline{\varphi}$ have to alternately exchange their roles, within $\underline{\underline{KS}}^{\underline{\varphi}}_{S(p,\nu)}$ and $\underline{\underline{KS}}^{\underline{\psi}}_{S(-p,-\nu)}$ or $\underline{\underline{KS}}^{\varpi(\underline{\varphi})}_{S(p,\nu)}$. Its principle will be detailed in the next section. We remind that

$$\underline{\varphi}^H\,\underline{\underline{KS}}^{\underline{\psi}}_{S(p,\nu)}\,\underline{\varphi} = \underline{\psi}^H\,\underline{\underline{KS}}^{\underline{\varphi}}_{S(-p,-\nu)}\,\underline{\psi} = \varpi(\underline{\psi})^H\,\underline{\underline{KS}}^{\varpi(\underline{\varphi})}_{S(p,\nu)}\,\varpi(\underline{\psi}) \tag{7}$$

where $\varpi(\underline{\psi})$ and $\varpi(\underline{\varphi})$ are the time-reversal versions of $\underline{\psi}$ and $\underline{\varphi}$, respectively. The above equalities indicate that the useful signal power can be expressed as a quadratic form on $\underline{\psi}$ for a given $\underline{\varphi}$ and vice versa, in two ways. The first one results from the inversion of the scattering function in time and frequency and the interchange of the Tx/Rx waveforms roles. The second one keeps the scattering function, $S(p,\nu)$, unchanged but requires the interchange of the Tx/Rx waveforms along with their time inversion.

B. Average Interference Power

The interference term within the decision variable Λ_{00}, given by $I_{00} = \sum_{(m,n)\neq(0,0)} a_{mn} < \underline{\psi}_{00}, \underline{\tilde{\varphi}}_{mn} >$, results from the contribution of all other transmitted symbols a_{mn}, such that $(m,n) \neq (0,0)$. The mean power of P_I^h, taken over channel realizations, is given by

$$P_I = \mathbb{E}[P_I^h] = \frac{E}{||\underline{\varphi}||^2} \sum_{(m,n)\neq(0,0)} \mathbb{E}[| < \underline{\psi}_{00}, \underline{\tilde{\varphi}}_{mn} > |^2].$$

By reiterating the same derivation as the previous section, P_I, is equal to

$$P_I = E\ \frac{\underline{\psi}^H \underline{\underline{KI}}^{\varphi}_{S(p,\nu)} \underline{\psi}}{||\underline{\varphi}||^2} \tag{8}$$

where the interference Kernel matrix is expressed as

$$\underline{\underline{KI}}^{\varphi}_{S(p,\nu)} = \sum_{k=0}^{K-1} \pi_k \left(\sum_{(m,n)\neq(0,0)} \sigma_{p_k}(\varphi_{mn} \underline{\varphi}_{mn}^H) \right) \odot \underline{\underline{\Phi}}_{\nu_k}. \tag{9}$$

Since $P_I > 0$, the interference Kernel $\underline{\underline{KI}}^{\varphi}_{S(p,\nu)}$ is also a Hermitian positive-semidefinite matrix, where $\underline{\underline{KI}}^{\varphi}_{S(p,\nu)}$ and $\underline{\underline{KI}}^{\psi}_{S(-p,-\nu)}$ verify also the similar identities

$$\underline{\psi}^H \underline{\underline{KI}}^{\varphi}_{S(p,\nu)} \underline{\psi} = \underline{\varphi}^H \underline{\underline{KI}}^{\psi}_{S(-p,-\nu)} \underline{\varphi} = \varpi(\underline{\psi})^H\ \underline{\underline{KI}}^{\varpi(\varphi)}_{S(p,\nu)}\, \varpi(\underline{\psi}).$$

When combined with (7), the above identities enable us to optimize the Tx vector $\underline{\varphi}$ through a maximization of the SINR, for any arbitrary choice of the Rx vector $\underline{\psi}$.

C. Average Noise Power

The correlation between the two noise samples N_{mn} and N_{kl} can be expressed as

$$\begin{aligned} \mathbb{E}[N_{mn}^* N_{kl}] &= \mathbb{E}[< \underline{\psi}_{mn}, \underline{r} >^* < \underline{\psi}_{kl}, \underline{r} >] \\ &= \underline{\psi}_{kl}^H \mathbb{E}[\underline{n}\ \underline{n}^H]\ \underline{\psi}_{mn} \\ &= N_0\ < \underline{\psi}_{kl}, \underline{\psi}_{mn} >. \end{aligned} \tag{10}$$

We point out that the noise correlation is a very critical parameter, since it induces an important error in small packets, which will complicate the channel decoding and, hence, degrade the transmission quality. Consequently, when there are more than one optimal waveform, which maximize the SINR, it is wise to choose the waveform, which minimizes the noise correlation. Taking $(k,l) = (m,n)$ in the previous equation, the average power of the noise term, N_{kl}, has the following expression:

$$P_N = N_0 \left\| \underline{\psi}_{kl} \right\|^2 = N_0 \left\| \underline{\psi} \right\|^2. \tag{11}$$

D. SINR Expressions

1) SINR Expressions for POPS-OFDM: Based on the elementary expressions obtained in the previous sections, we deduce that the SINR can be expressed as follows:

$$\text{SINR} = \frac{P_S}{P_I + P_N} = \frac{\underline{\psi}^H\ \underline{\underline{KS}}^{\varphi}_{S(p,\nu)}\ \underline{\psi}}{\underline{\psi}^H\ (\underline{\underline{KI}}^{\varphi}_{S(p,\nu)} + \frac{||\varphi||^2}{\text{SNR}}\underline{\underline{I}})\ \underline{\psi}} \tag{12}$$

where $\text{SNR} = \frac{E}{N_0}$. This expression is valid for a general channel model. We notice that, by interchanging $\underline{\varphi}$ and $\underline{\psi}$ roles, i.e., by letting $\underline{\psi}$ to be the transmit waveform and $\underline{\varphi}$ to be the receive waveform, the resulting SINR remains unchanged, where the scattering function is inverted in time and frequency domains. In fact, using the previous identities in (12), the SINR can be written as

$$\text{SINR} = \frac{\underline{\varphi}^H\ \underline{\underline{KS}}^{\psi}_{S(-p,-\nu)}\ \underline{\varphi}}{\underline{\varphi}^H\ (\underline{\underline{KI}}^{\psi}_{S(-p,-\nu)} + \frac{||\varphi||^2}{\text{SNR}}\underline{\underline{I}})\ \underline{\varphi}}. \tag{13}$$

The above equation allows the optimization of the transmit waveform, given a particular choice of the receive waveform. Also, while maintaining the initial scattering function, $S(p,\nu)$, interchanging the transmitting and receiving waveforms and taking their time-inversed versions, $\varpi(\underline{\psi})$ and $\varpi(\underline{\varphi})$, we can express the SINR as

$$\text{SINR} = \frac{\varpi(\underline{\varphi})^H\ \underline{\underline{KS}}^{\varpi(\psi)}_{S(p,\nu)}\ \varpi(\underline{\varphi})}{\varpi(\underline{\varphi})^H\ (\underline{\underline{KI}}^{\varpi(\psi)}_{S(p,\nu)} + \frac{||\varpi(\psi)||^2}{\text{SNR}}\underline{\underline{I}})\ \varpi(\underline{\varphi})}. \tag{14}$$

While (12) is used in the optimization of $\underline{\psi}$, given $\underline{\varphi}$, both (13) and (14) could be used interchangeably in the optimization of $\underline{\varphi}$, given $\underline{\psi}$. Nevertheless, from an implementation point of view, (14) is more tractable, since it preserves the same form of the scattering function as in (16), without recourse to inversions in time delay and Doppler frequency. Indeed, in the implementation code, the same piece of code, used for (12), could be employed to implement (14), where the roles of $\underline{\psi}$ and $\underline{\varphi}$ are interchanged, with $\varpi(\underline{\psi})$ injected instead of $\underline{\psi}$, to obtain $\varpi(\underline{\varphi})$, the time reverse of the optimized transmit waveform $\underline{\varphi}$. Besides reducing programming complexity, when combined with (12), the alternative expression of the SINR in (14) implies that if a couple of Tx/Rx waveforms, $(\underline{\varphi}, \underline{\psi})$, achieves a given SINR, then the dual couple, $(\varpi(\underline{\psi}), \varpi(\underline{\varphi}))$, obtained by interchanging and time-reversing the Tx and Rx waveforms, achieves the same SINR value. Additionally, if the couples $(\underline{\varphi}, \underline{\psi})$ and $(\varpi(\underline{\psi}), \varpi(\underline{\varphi}))$ are different, the couple leading to the least noise correlation at the Rx is preferable from an error correction point of view and should be adopted in practice. This observation also holds for the dual versions, CP-OFDM and zero-padding OFDM (ZP-OFDM), of conventional OFDM, where CP-OFDM is preferred to ZP-OFDM, since it is alone to offer a noise-correlation-free communication. When the pair $(\underline{\varphi}, \underline{\psi})$ offers a unique global maximum of the SINR, then the dual pairs, $(\underline{\varphi}, \underline{\psi})$ and $(\varpi(\underline{\psi}), \varpi(\underline{\varphi}))$, are identical, up to a pure complex multiplicative phase coefficient. Hence, up to an arbitrary phase shift, we have $\varpi(\underline{\varphi}) = \underline{\psi}$, which means that the transmit waveform $\underline{\varphi}$ and the receive waveform $\underline{\psi}$ are reversed time of each other. This behavior will be confirmed in the numerical results section, where all found pairs of optimized waveforms exhibit this time-reversal symmetry.

2) SINR Expression for Conventional OFDM: In the previous section, we derived the general expression of the SINR of any multicarrier system, including conventional OFDM, with its CP-OFDM and ZP-OFDM versions. This expression is next used to derive the achievable SINR by any dual forms of conventional OFDM. We recall that the transmit waveform $\underline{\varphi}^c$ and receive waveform $\underline{\psi}^c$ for CP-OFDM have rectangular forms with respective supports $[-(N-Q),\ldots,0,\ldots,(Q-1)]$ and $[0,\ldots,(Q-1)]$, and amplitudes $\frac{1}{\sqrt{N}}$ and $\frac{1}{\sqrt{Q}}$. We also recall that the transmit waveform $\underline{\varphi}^z$ and receive waveform $\underline{\psi}^z$ for ZP-OFDM have rectangular forms with respective supports $[0,\ldots,(N-1)]$ and $[0,\ldots,(Q-1)]$, and amplitudes $\frac{1}{\sqrt{N}}$ and $\frac{1}{\sqrt{Q}}$. With respect to (14), we emphasize that CP-OFDM and ZP-OFDM are duals of each other and lead to the same SINR, while, with respect to noise correlation, it is preferable to use CP-OFDM, since it guarantees zero correlation compared to ZP-OFDM.

As the receive waveforms of the CP-OFDM and ZP-OFDM, excluding the CP and ZP, respectively, constitute orthonormal bases, it results that the sum of the useful power (5) and the interference power (8) is equal to

$$P_S^c + P_I^c = \frac{E}{||\underline{\varphi}^c||^2} \sum_{(m=0,\ldots,Q-1,n)} \mathbb{E}[|<\underline{\psi}_{00}^c, \underline{\tilde{\varphi}}_{mn}^c>|^2] = E\frac{Q}{N}.$$

Consequently, the resulting SINR for CP-OFDM, denoted by SINR^c, is expressed as follows:

$$\text{SINR}^c = \frac{\frac{P_S^c}{E}}{\frac{Q}{N} - \frac{P_S^c}{E} + \frac{1}{\text{SNR}}}. \tag{15}$$

By injecting $\underline{\varphi}^c$ in (6), $\underline{\underline{KS}}_{S(p,\nu)}^{\underline{\varphi}^c}$ is expressed as

$$\underline{\underline{KS}}_{S(p,\nu)}^{\underline{\varphi}^c} = \begin{pmatrix} \frac{1}{N} & \cdots & \sum_{k=0}^{K-1}\gamma_k(N-p_k-1) \\ \sum_{k=0}^{K-1}\gamma_k(-1) & \cdots & \sum_{k=0}^{K-1}\gamma_k(N-p_k-2) \\ \vdots & \ddots & \vdots \\ \sum_{k=0}^{K-1}\gamma_k(-N+p_k+1) & \cdots & \frac{1}{N} \end{pmatrix}$$

where $\gamma_k(x) = \frac{\pi_k}{N} e^{j2\pi\nu_k T_s x}$. Hence, the power of the symbol of interest, P_S^c, is equal to (16) shown at the bottom of this page.

IV. POPS-OFDM Optimization Algorithm

As previously mentioned, the POPS-OFDM principle consists of alternating between an optimization of the transmit waveform $\underline{\varphi}$, given the receive waveform $\underline{\psi}$, and the optimization of the receive waveform $\underline{\psi}$, given the transmit waveform $\underline{\varphi}$. Precisely, this principle recalls in many respects the behavior of the famous Lloyd–Max algorithm [16], [17], which is used in optimum scalar or vector quantization design. Indeed, the Lloyd–Max algorithm iteratively alternates between an optimization of the codebook of representative vectors (in the multidimensional case) or points (in the unidimensional case), given all quantization regions, and vice versa. As the ping-pong keyword recalls, such a behavior is also observed in POPS-OFDM, which also alternates between two steps.

1) *The ping step:* This step starts the kth iteration by assuming the transmit waveform, $\underline{\varphi}^{(k-1)}$, to be available from the previous $(k-1)$th iteration. It optimizes the receive waveform $\underline{\psi}$ at the kth iteration according to

$$\underline{\psi}^{(k)} = \arg\max_{\underline{\psi}} \frac{\underline{\psi}^H \, \underline{\underline{KS}}_{S(p,\nu)}^{\underline{\varphi}^{(k-1)}} \, \underline{\psi}}{\underline{\psi}^H \, \underline{\underline{KIN}}_{S(p,\nu)}^{\underline{\varphi}^{(k-1)}} \, \underline{\psi}} \tag{17}$$

with $\underline{\underline{KIN}}_{S(p,\nu)}^{\underline{\varphi}} = \underline{\underline{KI}}_{S(p,\nu)}^{\underline{\varphi}} + \frac{||\underline{\varphi}||^2}{\text{SNR}} \underline{\underline{I}}$.
Since $\underline{\underline{KS}}_{S(p,\nu)}^{\underline{\varphi}}$ and $\underline{\underline{KI}}_{S(p,\nu)}^{\underline{\varphi}}$ are Hermitian and positive-semidefinite matrices, the optimization in (17) amounts to a maximization of a generalized Rayleigh quotient problem [18]. Consequently, since $\underline{\underline{KIN}}_{S(p,\nu)}^{\underline{\varphi}}$ is invertible for finite values of the SNR, as can be figured out from its expression above, the optimization problem becomes a maximization one, where the solution corresponds to the eigenvector of $(\underline{\underline{KIN}}_{S(p,\nu)}^{\underline{\varphi}})^{-1} \, \underline{\underline{KS}}_{S(p,\nu)}^{\underline{\varphi}}$ with the maximum eigenvalue.

2) *The pong step:* At this second and last step of the kth iteration, the optimized receive waveform $\underline{\psi}^{(k)}$ resulting from the ping step, is assumed to be available. Then, a time reversal transformation, $\varpi(\underline{\psi}^{(k)})$, of $\underline{\psi}^{(k)}$ is deduced. After that, based on (14), at the kth iteration, an optimization of $\varpi(\underline{\varphi})$ leading to $\varpi(\underline{\varphi}^{(k)})$, and consequently to the transmit waveform, $\underline{\varphi}^{(k)}$, by time inversion, is carried according to

$$\varpi(\underline{\varphi})^{(k)} = \arg\max_{\varpi(\underline{\varphi})} \frac{\varpi(\underline{\varphi})^H \, \underline{\underline{KS}}_{S(p,\nu)}^{\varpi(\underline{\psi}^{(k)})} \, \varpi(\underline{\varphi})}{\varpi(\underline{\varphi})^H \, \underline{\underline{KIN}}_{S(p,\nu)}^{\varpi(\underline{\psi}^{(k)})} \, \varpi(\underline{\varphi})} \tag{18}$$

with $\underline{\underline{KIN}}_{S(p,\nu)}^{\varpi(\underline{\psi}^{(k)})} = \underline{\underline{KI}}_{S(p,\nu)}^{\varpi(\underline{\psi}^{(k)})} + \frac{||\varpi(\underline{\psi})||^2}{\text{SNR}} \underline{\underline{I}}$. Here too, $\underline{\underline{KS}}_{S(p,\nu)}^{\varpi(\underline{\psi}^{(k)})}$ and $\underline{\underline{KI}}_{S(p,\nu)}^{\varpi(\underline{\psi}^{(k)})}$ are Hermitian and positive-semidefinite matrices. Consequently, the optimization considerations in the ping step hold, and the optimization problem in (18) amounts to a maximization of another generalized Rayleigh quotient problem,

$$P_S^c = E \begin{cases} \sum_{k=0}^{K-1}\gamma_k(0) + \sum_{k=0}^{K-1}\sum_{l=1}^{Q-1}\frac{2(Q-l)}{Q}\Re(\gamma_k(l)), & \text{if } \max_{k=0,\ldots,K-1} p_k \le N-Q \\ \sum_{k=0}^{K-1}\frac{N-p_k}{Q}\gamma_k(0) + \sum_{k=0}^{K-1}\sum_{l=1}^{N-p_k-1}\frac{2(N-p_k-l)}{Q}\Re(\gamma_k(l)), & \text{if } \max_{k=0,\ldots,K-1} p_k \le N. \end{cases} \tag{16}$$

where the solution corresponds to the eigenvector of $(\underline{\underline{KIN}}^{\varpi(\underline{\psi}^{(k)})}_{S(p,\nu)})^{-1}\ \underline{\underline{KS}}^{\varpi(\underline{\psi}^{(k)})}_{S(p,\nu)}$ with the maximum eigenvalue.

V. Upper Bound of the POPS-OFDM SINR

As we mentioned before, POPS-OFDM is an iterative algorithm permitting a systematic construction of the optimal waveforms at Tx/Rx sides. Unfortunately, the POPS-OFDM algorithm may be trapped in a local maximum, if the initialization waveform is not carefully chosen. Hence, an initialization step becomes necessary to guarantee a high SINR value. However, it is crucial to get an idea about the maximum SINR value. In order to derive the SINR upper bound, we reformulate the SINR expression (12) as follows:

$$\text{SINR} = \frac{(\underline{\varphi}\otimes\underline{\psi})^H\ \underline{\underline{A}}_{S(p,\nu)}\ (\underline{\varphi}\otimes\underline{\psi})}{(\underline{\varphi}\otimes\underline{\psi})^H\ \underline{\underline{B}}_{S(p,\nu)}\ (\underline{\varphi}\otimes\underline{\psi})} \tag{19}$$

where $\underline{\underline{A}}_{S(p,\nu)} = \sum_{k=0}^{K-1}\underline{\underline{\Omega}}_k^{(00)}$ and $\underline{\underline{B}}_{S(p,\nu)} = \sum_{(m.n)\neq(0,0)}\sum_{k=0}^{K-1}\underline{\underline{\Omega}}_k^{(mn)}$, with $\forall\quad m,n\in\mathbb{Z}$, $\underline{\underline{\Omega}}_k^{(mn)} = \underline{\underline{U}}^{m\ T}_{p_k+nN}\ \underline{\underline{\Pi}}_k^m\ \underline{\underline{U}}^m_{p_k+nN}$, $\underline{\underline{\Pi}}_k^m = [\pi_k\ e^{j2\pi(\nu_k T_s+\frac{m}{Q})(q-q')}]_{q,q'\in\mathbb{Z}}$ and

$$[\underline{\underline{U}}_d^m]_{qq'} = \begin{cases}1, & \text{if } q\ \bmod\ (d+mDN)=0 \quad \forall\, q'\in\mathbb{Z}\\ 0, & \text{else.}\end{cases}$$

In order to determine the SINR upper bound, $\overline{\text{SINR}}$, we have to maximize the SINR expression (19) over the Kronecker product between $\underline{\psi}$ and $\underline{\varphi}$, denoted by $\underline{\chi} = \underline{\varphi}\otimes\underline{\psi} = [\varphi_q\underline{\psi}]_{q\in\mathbb{Z}}$. By removing the restriction on $\underline{\chi}$ from the Kronecker product and letting freely span the whole space, an SINR maximization leads to

$$\overline{\text{SINR}} = \max_{\underline{\chi}}\ \frac{\underline{\chi}^H\ \underline{\underline{A}}_{S(p,\nu)}\ \underline{\chi}}{\underline{\chi}^H\ \underline{\underline{B}}_{S(p,\nu)}\ \underline{\chi}}. \tag{20}$$

Since $\underline{\underline{A}}_{S(p,\nu)}$ and $\underline{\underline{B}}_{S(p,\nu)}$ are Hermitian and positive semidefinite, the maximization problem in (20) becomes a straightforward maximization of a generalized Rayleigh quotient. Hence, $\overline{\text{SINR}}$ corresponds to the maximum eigenvalue of $\underline{\underline{B}}^{-1}_{S(p,\nu)}\ \underline{\underline{A}}_{S(p,\nu)}$.

VI. Characterization of POPS Waveforms

For the characterization of the waveforms, a radio channel, where the scattering function $S(p,\nu)$ has a multipath power profile with an exponential truncated decaying model and classical Doppler spectrum, is considered. Let $0<b<1$ be the decaying factor, such that the paths powers can be expressed as $\pi_k = \frac{1-b}{1-b^K}b^k$. Since sampled signals used at the Rx, a sampled channel in the time domain is also used, and therefore, the Doppler spectral density, denoted by $\alpha(\nu)$, is periodic in the frequency domain with period $\frac{1}{T_s}$. This scattering function follows the Jakes model that is decoupled from the dispersion in the time domain denoted as $\beta(p)$. As a result, $S(p,\nu)=\beta(p)\alpha(\nu)$, such as $\beta(p)=\sum_{k=0}^{K-1}\pi_k\delta_K(p-p_k)$ and

$$\alpha(\nu) = \begin{cases}\dfrac{2}{\pi B_d}\dfrac{1}{\sqrt{1-\left(\dfrac{2\nu}{B_d}\right)^2}}, & \text{if } |\nu|<\dfrac{B_d}{2}\\ 0, & \text{if } \dfrac{B_d}{2}\le|\nu|\le\dfrac{1}{2T_s}\end{cases} \tag{21}$$

where B_d is the Doppler spread. Hence, the useful and the interference Kernel matrices, derived in (6) and (9), will be expressed, respectively, as follows:

$$\underline{\underline{KS}}^{\varphi}_{S(p,\nu)} = \sum_{k=0}^{K-1}\pi_k\sigma_{p_k}(\underline{\varphi}\underline{\varphi}^H)\odot\underline{\underline{\Phi}} \tag{22}$$

$$\underline{\underline{KI}}^{\varphi}_{S(p,\nu)} = \left(\sum_n\sigma_{nN}\left(\sum_{k=0}^{K-1}\pi_k\sigma_{p_k}(\underline{\varphi}\underline{\varphi}^H)\right)\odot\underline{\underline{\Omega}}\right) - \underline{\underline{KS}}^{\varphi}_{S(p,\nu)} \tag{23}$$

where $\underline{\underline{\Phi}}$ and $\underline{\underline{\Omega}}$ are the Hermitian matrices for the useful and the interference Kernel matrices expressed, respectively, as follows:

$$\underline{\underline{\Phi}} = \left[\int_\nu\alpha(\nu)e^{j2\pi\nu T_s(q-p)}\right]_{pq} = [J_0(\pi B_d T_s(p-q))]_{pq} \tag{24}$$

and $\underline{\underline{\Omega}} = [\Omega_{pq}]_{pq}$ with

$$\Omega_{pq} = \begin{cases}QJ_0(\pi B_d T_s(p-q)), & \text{if } (p-q)\bmod Q=0\\ 0, & \text{else.}\end{cases}$$

Hence, for the same context, the SINR expression for the conventional OFDM remains identical to (15), where the useful power, P_S^c, is equal to (25) shown at the bottom of this page.

A. Implementation of the POPS-OFDM Algorithm

In this section, we put emphasis on the main added values of the POPS-OFDM algorithm, related to the implementation aspects.

1) Discrete-time versions of the transmit and receive waveforms are considered from the start, avoiding any further discretization step, which, otherwise, typically occurs a degradation in the original optimized performance.
2) Finite duration supports of the transmit and receive waveforms are used in the optimization process, avoiding any need for truncation prior to any actual implementation step, circumventing any SINR degradation.

In the following, it will become clear for the reader that the use of finite duration supports for the Tx and Rx waveforms will

$$P_S^c = \frac{E}{NQ}\begin{cases}Q+\sum_{l=1}^{Q-1}2(Q-l)J_0(\pi B_d T_s l), & \text{if } \max_{k=0\ldots K-1}p_k\le N-Q\\ \sum_{k=0}^{K-1}\pi_k(N-p_k)+\sum_{k=0}^{K-1}\pi_k\sum_{l=1}^{N-p_k-1}2(N-p_k-l)J_0(\pi B_d T_s l), & \text{if } \max_{k=0\ldots K-1}p_k\le N.\end{cases} \tag{25}$$

lead to an exact computation of the Kernel matrices involved in the optimization process.

1) POPS-OFDM With Equal Tx/Rx Waveform Durations: Typically, the same duration for both transmit and receive waveforms is used in practice, i.e., $D_{\underline{\psi}} = D_{\underline{\varphi}} = D$. In this case, the implementations of the ping and pong steps are the same. Therefore, only the case of the ping step is explained next. As illustrated in Fig. 2, given the transmit waveform vector $\underline{\varphi}$, the search for the optimum receive waveform vector $\underline{\psi}$ only requires finite $D \times D$ submatrices of the interference Kernel, $\underline{\underline{KI}}^{\underline{\varphi}}_{S(p,\nu)}$, and the useful Kernel, $\underline{\underline{KS}}^{\underline{\varphi}}_{S(p,\nu)}$. As such, only a finite number of time shifts of the matrix $\underline{\varphi}\underline{\varphi}^H$ is involved in the full specification of this submatrix, and consequently, the summation (23) could be restricted to a finite number of terms. This restriction allows the exact computation of the SINR, with reduced complexity, and without any recourse to approximations. According to Fig. 2, matrix $\underline{\varphi}\underline{\varphi}^H$ is first shifted according to the multipath power profile. Then, the resulting aggregate matrix is, in turn, repeatedly shifted by integer multiples of the normalized symbol duration, N. As partially shown in Fig. 2, the useful and interference kernels needed in the optimization of $\underline{\varphi}$ and $\underline{\psi}$ are delimited by two square selection windows. Nevertheless, since the channel is dispersive and causal, the selection window for $\underline{\psi}$ should be diagonally shifted by around the average incurred delay, with respect to the selection window of $\underline{\varphi}$, to capture most of the achievable SINR.

2) POPS-OFDM With Different Tx/Rx Waveform Durations: When optimizing Tx/Rx waveforms, using POPS-OFDM, we should not forget about the possible use of these waveforms in a multiple access fashion. In this practical framework, interferences incurred by other simultaneous transmission should be kept at minimum, especially in the uplink, where power unbalance and frequency and time misalignment are commonplace [19], [20]. These interferences could be caused by the cumulative effects of amplification nonlinearities and nonideal filtering, at the Tx side, and nonideal filtering, at the Rx side [19]. Contribution to these interferences, from the Tx side, are measured by the adjacent channel leakage power ratio (ACLR) [19], which is defined as the ratio of the in-band transmitted power to the power measured in an adjacent channel. From the Rx side, these contributions are measured by the adjacent channel selectivity (ACS) [20], which is a measure of the Rx's ability to filter out the power transmitted on an adjacent channel band. A poor ACS performance may lead to dropped calls in certain areas of the cells, also called dead zones [19]. To achieve an increased immunity to both Tx and Rx sources of multiple access interference, it is recommended to use large Tx and Rx waveform durations to increase as much as possible the ACLR and the ACS, respectively. Unfortunately, any increase in the waveform duration at any side not only incurs an increase in processing complexity, but also leads to an increase in latency, which could turn to be harmful for some applications and services. Nevertheless, the transmit and receive waveforms durations could still be taken different to better adapt to the disparity in computational capabilities between Tx and Rx sides, while reducing as much as possible multiple access interference. The POPS-OFDM paradigm can easily be extended to the optimization of Tx and Rx waveforms with different durations. However, its implementation is slightly different compared to the case of equal waveforms durations. For the illustration sake, we next consider the case where $D_{\underline{\psi}} > D_{\underline{\varphi}}$. The case where $D_{\underline{\psi}} < D_{\underline{\varphi}}$ could be treated in the same way. The ping and pong steps for $D_{\underline{\psi}} > D_{\underline{\varphi}}$ are implemented as follows.

1) *The ping step:* Since, in the kth iteration, $\underline{\varphi}^{(k-1)}$ is available, $\underline{\psi}$ is optimized according to (17). As depicted in Fig. 3(a), matrix $\underline{\varphi}\underline{\varphi}^H$ is shifted, according to the channel multipath power profile. Afterward, the obtained matrix is shifted repetitively, every normalized symbol duration, N [see Fig. 3(a)]. Then, the useful and interference kernels for the optimization of $\underline{\psi}$ are extracted according to the square selection window of $\underline{\psi}$. Again, to achieve the best maximized SINR, the selection window for $\underline{\psi}$ should roughly be shifted with respect to that of $\underline{\varphi}$ by the average channel delay.
2) *The pong step:* At this step, $\underline{\psi}^{(k)}$ is available from the ping step. First, a time-reversal transformation, $\varpi(\underline{\psi}^{(k)})$, of $\underline{\psi}^{(k)}$ is deduced. Then, based on (14), an optimization of $\varpi(\underline{\varphi})$ is accomplished, leading to $\varpi(\underline{\varphi}^{(k)})$ and, therefore, to $\underline{\varphi}^{(k)}$ by time inversion. We notice that the pong step has the same principle as the ping one. However, here, the square selection windows, specifying the useful and interference Kernels of $\underline{\varphi}$ and $\underline{\psi}$, are $D_{\underline{\varphi}} \times D_{\underline{\varphi}}$ and $D_{\underline{\psi}} \times D_{\underline{\psi}}$, respectively, and could therefore be different [see Fig. 3(b)].

It should also be noted that this diagonal shift is of utmost importance for reduced duration Tx and Rx waveforms (comparable to the symbol period), since the SINR is strongly dependent on, due to reduced degrees of freedom in the waveform design. For Tx and Rx waveforms, with large durations (several times larger than the symbol period), variations of the achievable SINR around the optimum window shift are of less importance, since there is room for an additional artificial correction shift that could be achieved within the support of $\underline{\psi}$, thanks to the higher degrees of freedom offered for the waveform design.

B. POPS-OFDM Performance

In this section, we consider multiple metrics to illustrate the performance of POPS-OFDM. As mentioned before, the channel is characterized by the Doppler spread (B_d) and the delay spread (T_m). The sensitivity of the multicarrier system to the Doppler spread is measured by the normalized Doppler spread factor ($\frac{B_d}{F}$). In fact, when the subcarrier spacing, F, is big for a given Doppler spread value, B_d, the system is less sensitive to Doppler dispersion. Likely, the sensitivity of the multicarrier system to the delay spread is measured by the normalized delay spread factor ($\frac{T_m}{T}$), where T is the symbol period. Yet, the product (FT), which is the inverse of the time-frequency lattice density, is fixed for a given spectral efficiency. Hence, we cannot increase simultaneously and freely both F and T values in order to reduce system sensitivity to Doppler and delay spreads. Consequently, a compromise between the normalized frequency

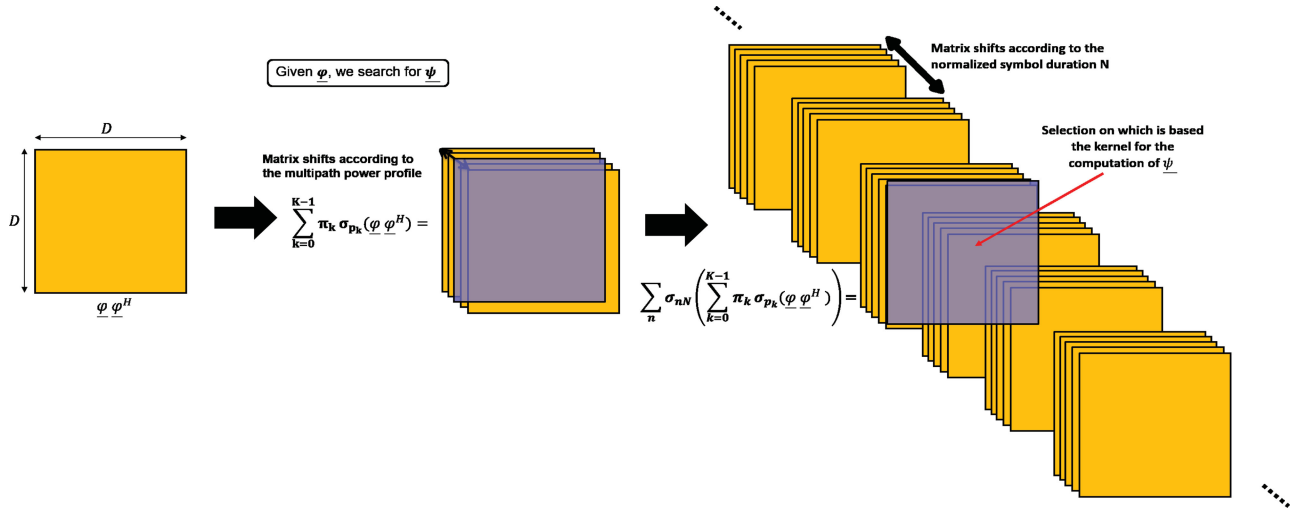

Fig. 2. POPS-OFDM implementation methodology, taking into account the channel Doppler spread and the lattice periodic structure in time.

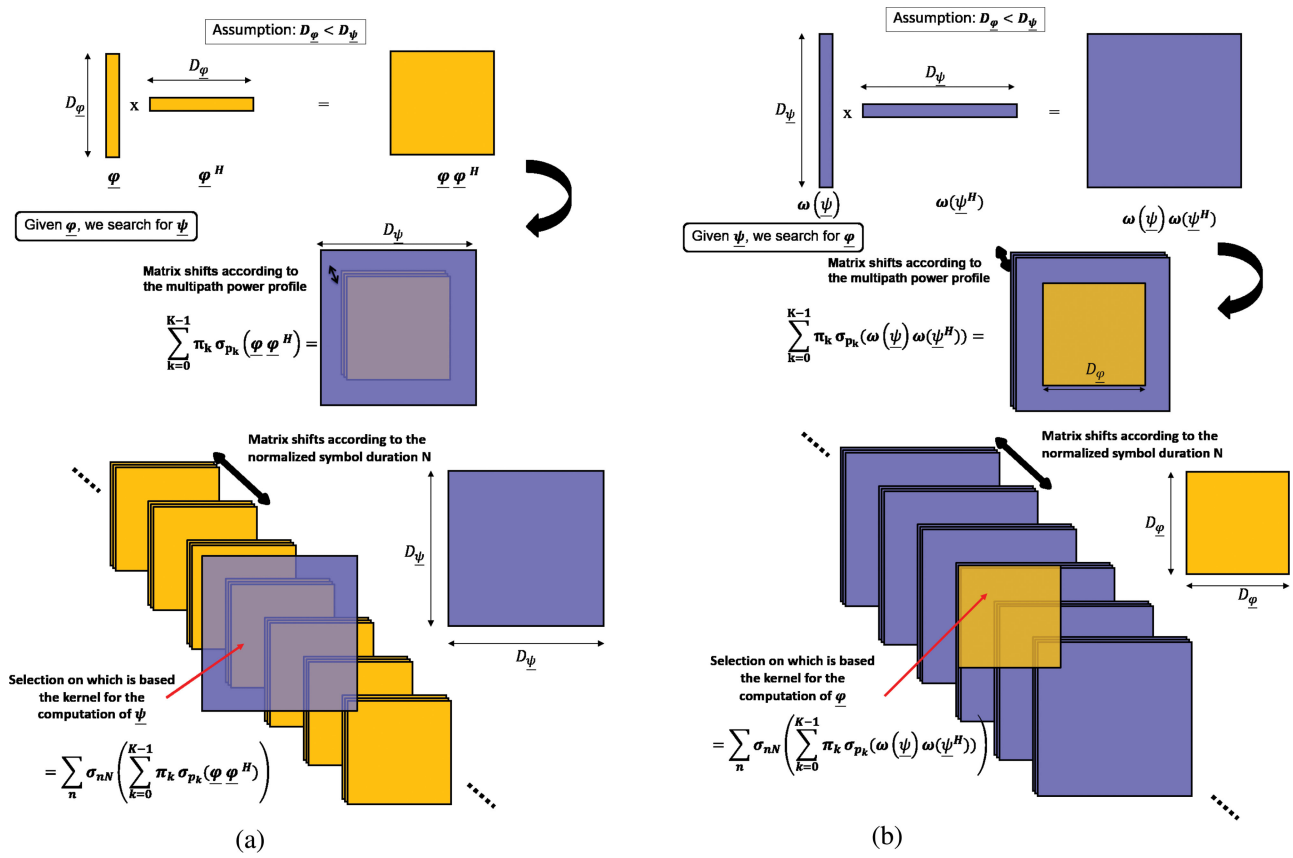

Fig. 3. POPS-OFDM implementation methodology, taking into account the lattice periodic structure and repetitive structure in time and the channel Doppler spread. (a) Ping step ($D_{\underline{\psi}} > D_{\underline{\varphi}}$). (b) Pong step ($D_{\underline{\psi}} > D_{\underline{\varphi}}$).

spread factor ($\frac{B_d}{F}$) and the normalized time spread factor ($\frac{T_m}{T}$) should be found. If this is the case, we can say that the system is balanced. To do so, we illustrate in Fig. 4 the SINR versus ($\frac{B_d}{F}$), and then, we determine the adequate values of ($\frac{B_d}{F}$), for a given values of $B_d T_m = 0.01$ and for both $FT = 1.0625$ $(N = 136)$ and $FT = 1.25$ $(N = 160)$, that correspond to the optimum balancing. In this figure, we also compare the performance of POPS-OFDM and conventional OFDM, with CP of eight or 32 samples. The obtained results prove that POPS-OFDM outperforms conventional OFDM systems.

Fig. 5 illustrates the evolution of the signal-to-interference ratio (SIR) versus FT, for both conventional OFDM and POPS-OFDM, for different waveform durations. As expected, we note that whatever the support duration of the Tx/Rx waveforms,

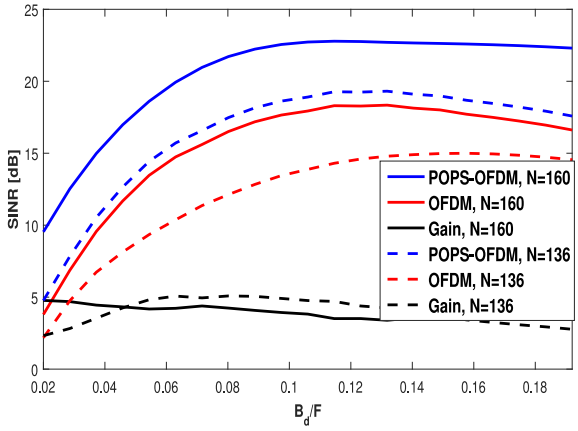

Fig. 4. Doppler spread-delay spread balancing ($Q = 128$ and $D = 3N$).

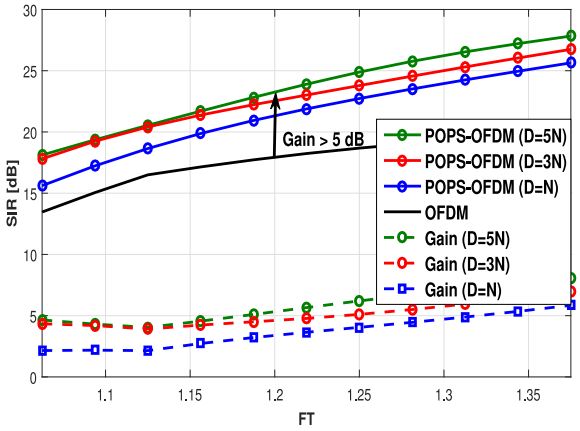

Fig. 5. Performance and gain in the SIR. Identical Tx/Rx waveform durations.

the proposed system always outperforms conventional OFDM for a large range of channel dispersions, especially for a highly frequency dispersive channel. This figure reveals a significant SIR increase, reaching as much as 8 dB, as the support duration increases. Furthermore, it represents a mean to deduce the adequate couple, (T, F), which ensures the best compromise between Doppler and delay spreads. We note that for a lattice density equivalent to $FT = 1.25$, corresponding to a conventional OFDM system with a CP having a one-quarter of the time symbol duration, the SIR achieved by POPS-OFDM, for $D = N$, exceeds 4 dB the one obtained by conventional OFDM.

The optimized Tx/Rx waveform shapes are illustrated in Fig. 6 for $FT = 1.25$ and $B_d T_m = 0.01$. We remark that the Tx/Rx waveform shapes are different from those of conventional OFDM.

Fig. 7 shows that the obtained Tx waveform reduces the OOB emissions, by about 80 dB, contrarily to conventional OFDM, and it avoids the need of large guard bands. In this figure, we observe that the optimal prototype waveforms are well localized in the frequency domain, and the gain becomes less pronounced when $D \geq 5N$.

Fig. 8 presents the behavior of the SIR with respect to FT for different Tx/Rx waveform durations, where we proceed by

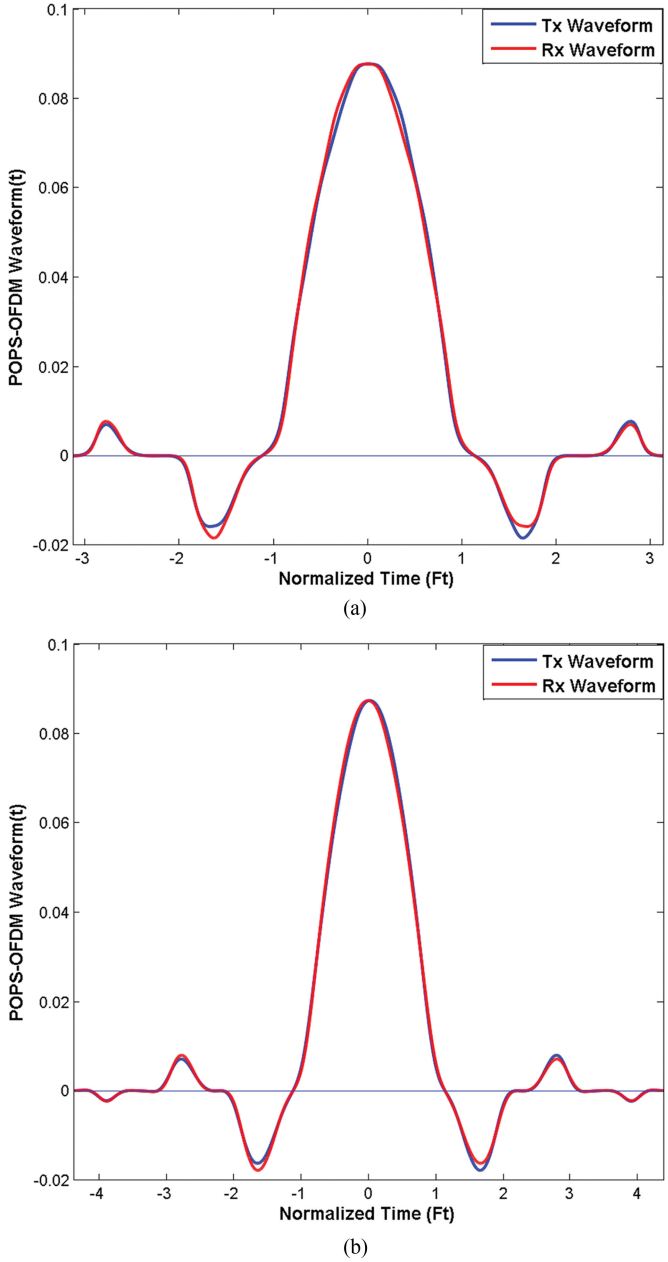

Fig. 6. POPS optimized waveforms. (a) $D = 5N$. (b) $D = 7N$.

fixing the Tx waveform duration and increasing gradually the Rx waveform duration. As expected, this figure shows that an increase of Rx waveform durations with respect to the Tx waveform duration leads to a slight increase in the SIR.

C. SIR Dependence to Waveform Initialization

We emphasize that POPS-OFDM banks on an iterative algorithm, and as a matter of fact, it is very sensitive to waveform initialization. Nevertheless, this issue should not make questionable, in any way, the significance and usefulness of the POPS algorithm. Indeed, vulnerability to initialization is encountered in several iterative, yet very useful and very famous, algorithms, such as the Lloyd–Max iterative algorithm, which can also con-

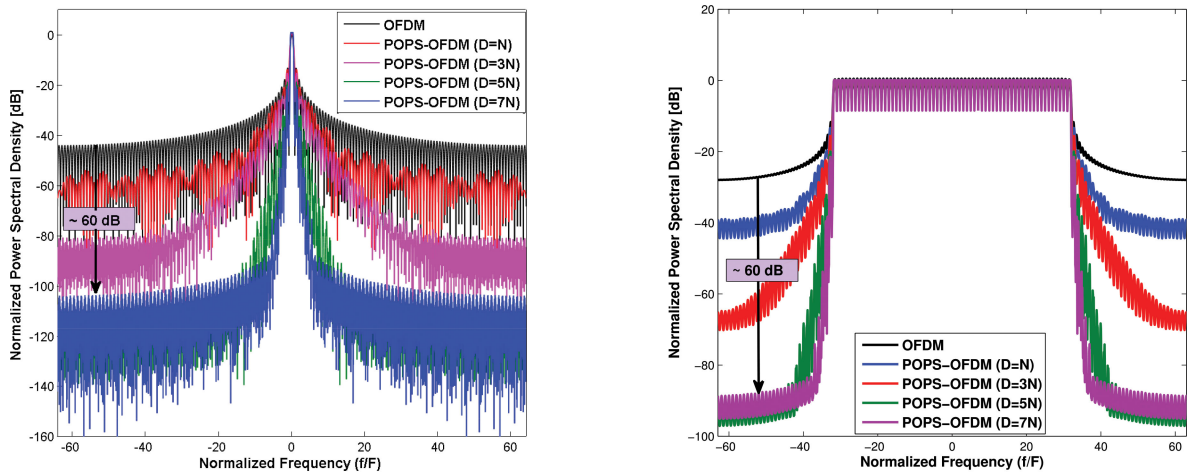

Fig. 7. Normalized power spectral density of POPS-OFDM compared to CP-OFDM. (a) Spectrum of one subcarrier. (b) Spectrum of 64 subcarriers.

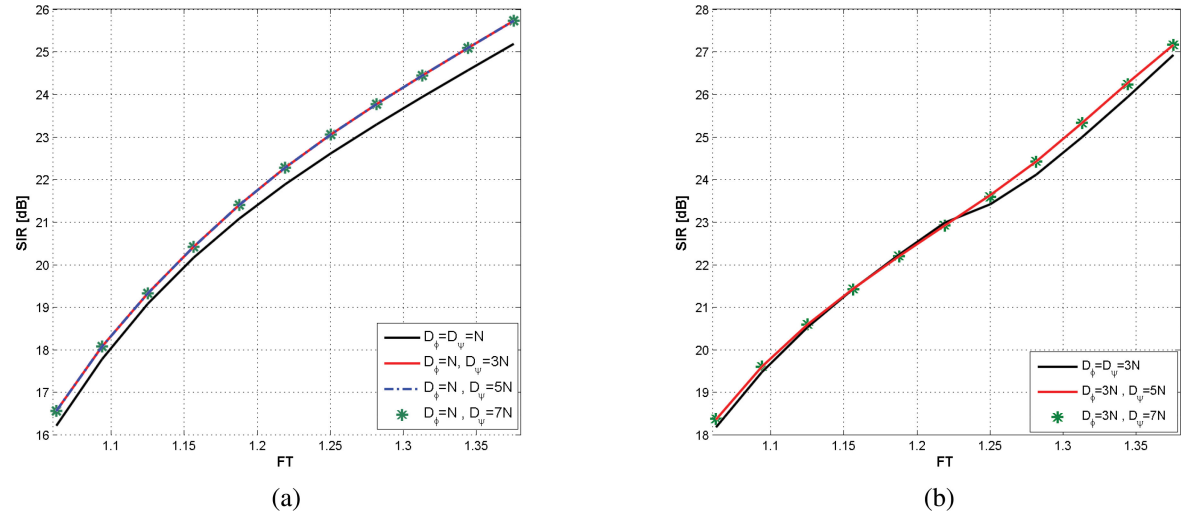

Fig. 8. Performance in SIR. Different Tx/Rx waveform durations. (a) $D_\varphi = N$. (b) $D_\varphi = 3N$.

verge to local minima of the quantization distortion cost function [16]. Motivated by the fact that the Hermite functions form an orthonormal base of the Hilbert space, $l^2(\mathbb{R})$, of square summable functions and offer the best localization in time and frequency domains in decreasing order, we initialize the POPS-OFDM algorithm with different linear combinations of time-sampled versions of the eight most localized Hermite functions. Furthermore, we consider Gaussian waveforms with various standard deviation values, in addition to the root-raised cosine waveforms, with different roll-off factors, during the initialization step [see Fig. 9(a)]. Other initialization waveforms could be envisaged, such as discrete prolate spheroidal sequences, Slepian sequences, and Mirabbasi–Martin waveforms based on cosine waveform expansions. Fig. 9 reveals the existence of local maxima in the SINR cost function to be maximized. Nevertheless, it also reveals that, most of the time, the POPS algorithm converges to SINR values larger than the one reached by conventional OFDM. Moreover, as expected, the best achieved SINR stays always below the SINR upper bound [see Fig. 9(b)]. For large values of D, the Kernel matrices involved in the expression of the upper bound, in (19), of size $D^2 \times D^2$, become very large, thus preventing any possible numerical evaluation. Consequently, in Fig. 9(b), only the SINR upper bound for $Q = 64$ and $D = N = 80$ is considered.

D. Robustness Characterization

So far, the performance of POPS-OFDM has been assessed for a perfect transmission conditions. Unfortunately, these perfect conditions are never met in practice, where some imperfections could seriously hamper the achieved SINR gains. This section precisely assesses the POPS-OFDM robustness to time and frequency synchronization errors, as well as to estimation errors in the channel statistics, characterized by the channel spreading factor, $B_d T_m$. Fig. 10(a) compares the robustness of POPS-OFDM and conventional OFDM in terms of time syn-

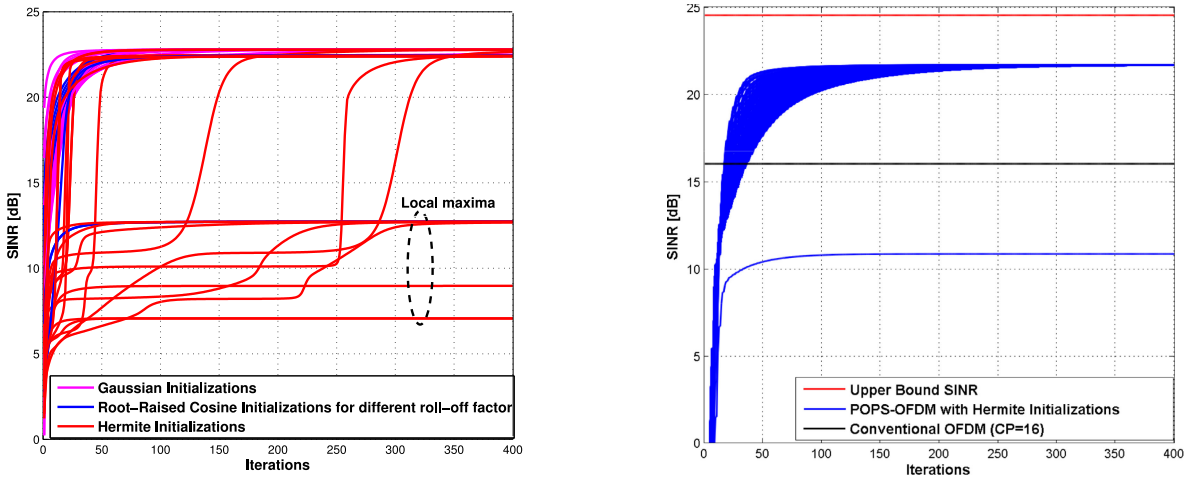

Fig. 9. Impact of different waveforms' prototype initializations. (a) $Q = 128, D = 3N$. (b) $Q = 64, D = N$.

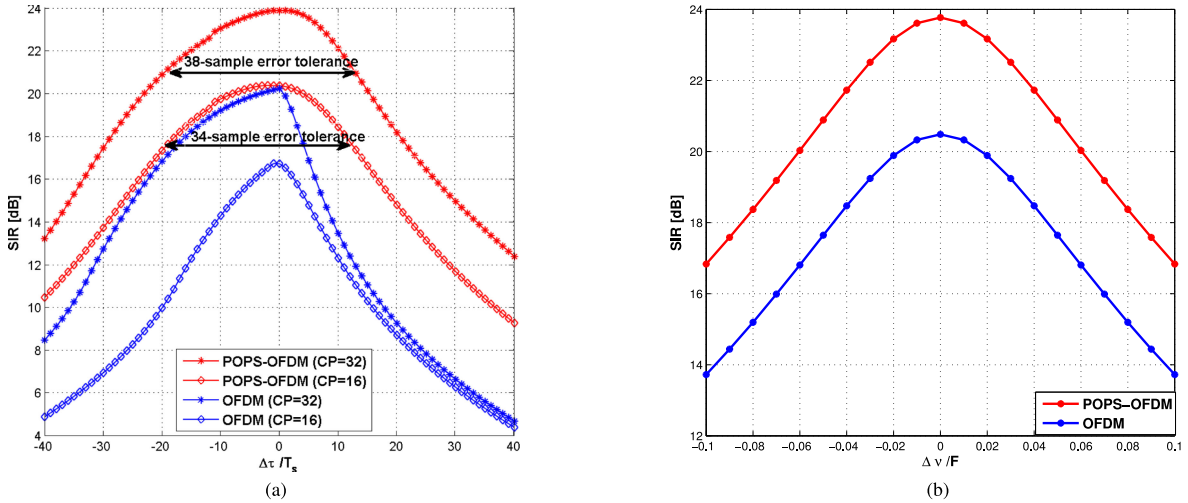

Fig. 10. Sensitivity to synchronization errors. (a) Time. (b) Frequency.

chronization errors, when $CP = 32$ and $CP = 16$. This figure confirms that POPS-OFDM is less sensitive to time synchronization errors than conventional OFDM. With regard to sensitivity to frequency synchronization errors, it could be noticed, from Fig. 10(b), that POPS-OFDM and conventional OFDM have practically the same behaviors. The computation of the Kernel matrices in the POPS algorithm assumes a perfect knowledge of the scattering function of the actual propagation channel. In practice, an indirect parametric estimation of this scattering function, through its channel spread factor, B_dT_m, should be carried during effective transmission. As a matter of fact, the optimized waveforms that are used during transmission cannot exactly be matched to the actual transmission statistical parameters. Fig. 11 quantifies the degradation in POPS-OFDM performance due to a mismatch between the values of B_dT_m characterizing the actual channel, on the one hand, and used for offline waveform optimization, on the other hand. This figure reveals that if B_dT_m varies in the range from 0.001 to 0.01, a wise choice is to use optimal Tx/Rx waveforms optimized for

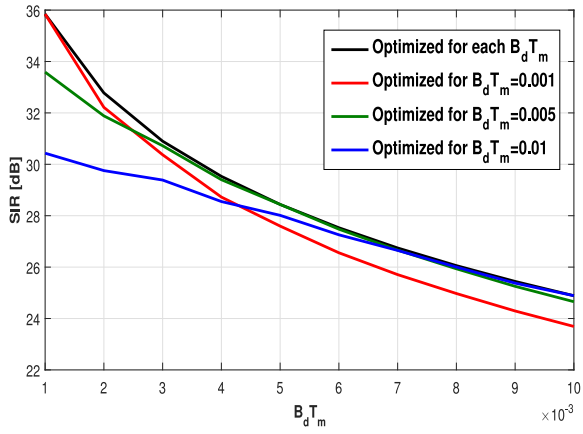

Fig. 11. POPS-OFDM sensitivity to estimation errors on B_dT_m.

$B_dT_m = 0.005$ to guarantee a slow SINR degradation. According to our cumulated experience, this observation is valid for

other ranges of $B_d T_m$, meaning that, in practice, we only need a finite codebook of optimized Tx/Rx waveform pairs, to be used in an adaptive way, to guarantee an insignificant degradation in the SINR performance.

VII. Conclusion

In this paper, we analyzed in detail the performance of the discrete-time POPS-OFDM optimum waveform design technique. We showed that POPS-OFDM allows an offline iterative waveform optimization at the Tx/Rx sides, which guarantees an important SINR increase compared to conventional OFDM. Moreover, we unveiled the capacity of POPS-OFDM waveforms to offer a dramatic reduction in OOB emissions, leading to a better use of the spectral resources, in multiple access scenarios. Furthermore, we have tested the robustness of POPS-OFDM waveforms against time synchronization errors and imperfect knowledge of the scattering function of the actual propagation channel. These benefits make POPS-OFDM waveforms competitive candidates for 5G systems. We believe that, thanks to the POPS paradigm, adaptive waveform communications will become part of 5G systems, side-by-side with other link adaptation techniques, such as fast power control and adaptive modulation and coding. A perspective of our research work could be an extension of the POPS optimization technique to multiple-input multiple-output systems. Another potential perspective could be the design of OFDM waveforms optimized for partial equalization, carrier aggregation, or low latency, with tolerance to bursty communications and relaxed synchronization.

References

[1] 3GPP, *RAN 5G Workshop*, 2015. [Online]. Available: http://www.3gpp.org/newsevents/3gpp-news/1734-ran_5G

[2] *On Study on New Radio NR Access Technology: Physical Layer Aspects*, Document RAN1 TR 38.802, Mar. 2017.

[3] Y. Medjahdi *et al.*, "On the road to 5G: Comparative study of physical layer in MTC context," *IEEE Access*, vol. 5, pp. 26556–26581, 2017.

[4] G. Wunder *et al.*, "5GNOW: Non-orthogonal, asynchronous waveforms for future mobile applications," *IEEE Commun. Mag.*, vol. 52, no. 2, pp. 97–105, Feb. 2014.

[5] F. Schaich *et al.*, "FANTASTIC-5G: 5G-PPP project on 5G air interface below 6 GHz," in *Proc. Eur. Conf. Netw. Commun.*, Jul. 2015, pp. 12–15.

[6] H. Lin and P. Siohan, "Major 5G waveform candidates: Overview and comparison," in *Signal Processing for 5G: Algorithms and Implementations*. New York, NY, USA: Wiley, 2016, pp. 169–188.

[7] N. Michailow *et al.*, "Generalized frequency division multiplexing: Analysis of an alternative multi-carrier technique for next generation cellular systems," in *Proc. Int. Symp. Wireless Commun. Syst.*, 2012, pp. 171–175.

[8] G. Fettweis, M. Krondorf, and S. Bittner, "GFDM—Generalized frequency division multiplexing," in *Proc. IEEE 69th Veh. Technol. Conf.*, 2009, pp. 1–4.

[9] M. Bellanger, "FBMC physical layer: A primer," ICT-PHYDYAS, Paris, France, Tech. Rep., Jun. 2010, pp. 1–31. [Online]. Available: http://www.ictphydyas.org/teamspace/internal-folder/FBMC-Primer_06-2010.pdf

[10] Y. H. Yun, C. Kim, K. Kim, Z. Ho, B. Lee, and J. Y. Seol, "A new waveform enabling enhanced QAM-FBMC systems," in *Proc. IEEE 16th Int. Workshop Signal Process. Adv. Wireless Commun.*, 2015, pp. 116–120.

[11] J.-B. Doré, V. Berg, and D. Kténas, "Channel estimation techniques for 5G cellular networks: FBMC and multiuser asynchronous fragmented spectrum scenario," *Trans. Emerg. Telecommun. Technol.*, vol. 26, pp. 15–30, Jan. 2015.

[12] V. Vakilian, T. Wild, F. Schaich, S. ten Brink, and J.-F. Frigon, "Universal-filtered multi-carrier technique for wireless systems beyond LTE," in *Proc. IEEE Globecom Workshops*, 2013, pp. 223–228.

[13] M. Siala, F. Abdelkefi, and Z. Hraiech, "Novel algorithms for optimal waveforms design in multicarrier systems," in *Proc. IEEE Wireless Commun. Netw. Conf.*, 2014, pp. 1270–1275.

[14] Z. Hraiech, F. Abdelkefi, and M. Siala, "POPS-OFDM: Ping-pong optimized pulse shaping-OFDM for 5G systems," in *Proc. IEEE Int. Conf. Commun.*, 2015, pp. 4781–4786.

[15] Z. Hraiech, F. Abdelkefi, M. Siala, and W. Ben-Ameur, "Characterization of ping-pong optimized pulse shaping-OFDM (POPS-OFDM) for 5G systems," in *Proc. IEEE 81st Veh. Technol. Conf.*, 2015, pp. 1–6.

[16] Q. Du, M. Emelianenko, and L. Ju, "Convergence of the Lloyd algorithm for computing centroidal Voronoi tessellations," *SIAM J. Numer. Anal.*, vol. 44, pp. 102–119, Jan. 2006.

[17] Z. Peric and J. Nikolic, "An effective method for initialization of Lloyd-MAX's algorithm of optimal scalar quantization for Laplacian source," *Informatica*, vol. 18, pp. 279–288, 2007.

[18] R. E. Prieto, "A general solution to the maximization of the multidimensional generalized Rayleigh quotient used in linear discriminant analysis for signal classification," in *Proc. IEEE Int. Conf. Acoust., Speech, Signal Process.*, 2003, pp. VI-157–VI-160.

[19] H. Holma and A. Toskala, Eds., *WCDMA for UMTS: HSPA Evolution and LTE*, 4th ed. Chichester, U.K.: Wiley, 2007.

[20] *Radio Frequency (RF) System Scenarios (Release 13)*, Document 3GPP TR 25.942 (V13.0.0), 2016.

Authors' photographs and biographies not available at the time of publication.